

DOI:10.1002/ejic.201402964

Slow Magnetic Relaxation in Mononuclear Octahedral Manganese(III) Complexes with Dibenzoylmethanide Ligands

Lei Chen,^[a] Jing Wang,^[a] Yuan-Zhong Liu,^[a] You Song,^[a]
 Xue-Tai Chen,^{*[a]} Yi-Quan Zhang,^{*[b]} and Zi-Ling Xue^[c]

Keywords: Manganese / N,O ligands / Single-molecule magnets / Magnetic properties

The structural characterization and magnetic studies of three mononuclear Mn^{III} complexes based on the dibenzoylmethanido (dbm⁻) ligand, Mn(dbm)₃ (**1**) and [Mn(dbm)₂(L)₂](ClO₄) (L = dimethyl sulfoxide, **2**; L = pyridine, **3**), are reported. The Mn^{III} ions are in an axially elongated octahedral coordination geometry. The axial zero-field-splitting parameters *D*, ranging from -3.42 to -4.52 cm⁻¹ for the three complexes, were

obtained by fitting magnetic-susceptibility and magnetization data. Ab initio calculations also show the axial magnetic anisotropy in the molecules of **1–3**. With an applied dc field, the ac susceptibility measurements reveal slow magnetic relaxation in **1–3**. The possible relationship between the structures and the magnetic properties in these complexes are discussed.

Introduction

Superparamagnetic discrete molecules exhibit slow magnetic relaxation and other quantum properties, and they are known as single molecule magnets (SMMs).^[1] The slow magnetic relaxation of SMMs arises from the reversal of spin overcoming an energy barrier *U*, which is based on the ground-state spin *S* and the uniaxial anisotropy *D* with *U* = |*D*|*S*² for integer and *U* = |*D*|(*S*² - 1/4) for half-integer spins. Therefore, achieving a large spin value (*S*), increasing the uniaxial anisotropy (*D*), and the combination of these two approaches have been employed to increase the spin-reversal barrier and to improve the magnetic properties of SMMs. Initially, the study of SMMs had been focused on transition-metal clusters, especially on polynuclear Mn clusters,^[2] because it is easier to design and synthesize such clusters with a strong magnetic coupling between the metal centers than to control the anisotropy of a molecule. The family of SMMs has since been extended to polynuclear 3d-4f^[3] and lanthanide clusters^[4] by introducing lanthanide

ions with large magnetic anisotropies. Since Ishikawa et al.^[5] reported the first example of a mononuclear lanthanide-based SMM, so-called single-ion magnets (SIMs), the slow magnetic relaxation behavior has been observed in many mononuclear complexes containing lanthanide or actinide ions.^[6]

More recently, mononuclear complexes based on transition-metal ions have exhibited SMM behavior as well.^[7–11] Mononuclear Mn^{III} complexes are of particular interest, because the largest family of polynuclear SMMs contains the Mn^{III} ion. The d⁴ Mn^{III} ion has an ⁵E_g ground state in an octahedral environment, such that the first-order orbital contribution is quenched. However, because of the Jahn–Teller effect in octahedral, high-spin Mn^{III} complexes, the ⁵E_g ground state is split into ⁵A_{1g} and ⁵B_{1g}, which corresponds to an axial elongation with the zero-field-splitting (ZFS) parameter *D* < 0 in most cases or to an axial compression resulting in *D* > 0 in rare cases.^[12] Therefore, the highly elongated configuration attracted considerable attention in the search for new Mn^{III} SIMs with negative *D* values. So far, three samples of Mn^{III}-based SIMs have been reported. Ishikawa et al.^[11a] presented a Mn^{III}–salen-type complex with a diamagnetic [Co^{III}(CN)₆]³⁻ unit, [Mn{5-TMAM(*R*)-salmen}(H₂O)–Co(CN)₆}]·7H₂O·MeCN {5-TMAM(*R*)-salmen = (*R*)-*N,N'*-(1-methylethylene)bis[(5-trimethylammoniomethyl)salicylideneimine]}, which shows magnetic relaxation properties without frequency-dependent maxima in the frequency range 1–1500 Hz. Sanakis et al.^[11b] observed field-induced slow magnetic relaxation in the mononuclear octahedral manganese(III) complex [Mn{(OPPh₂)₂N}₃] with a frequency dependence of the out-of-phase ac susceptibility signals at the low temperature

[a] State Key Laboratory of Coordination Chemistry, Nanjing National Laboratory of Microstructures, School of Chemistry and Chemical Engineering, Nanjing University, Nanjing 210093, China
 E-mail: xtchen@netra.nju.edu.cn
<http://chem.nju.edu.cn/english/faculty/r.asp?fn=CHEN,Xuetai>

[b] Jiangsu Key Laboratory for NSLSCS, School of Physical Science and Technology, Nanjing Normal University, Nanjing 210023, China
 E-mail: zhangyiquan@njnu.edu.cn
http://physics.njnu.edu.cn/szdw/2014-10/111956_147489.html

[c] Department of Chemistry, University of Tennessee Knoxville, Tennessee 37996, USA

Supporting information for this article is available on the WWW under <http://dx.doi.org/10.1002/ejic.201402964>.

of 2.0 K, but no frequency-dependent maxima were found in the frequency range 1–10000 Hz. Vallejo et al.^[11c] have observed out-of-phase maxima at frequencies in the range 1–10000 Hz in the six-coordinate Mn^{III} complex (Ph₄P)[Mn(opbaCl₂)(py)₂] [H₄opbaCl₂ = *N,N'*-3,4-dichloro-*ortho*-phenylenebis(oxamic acid), Ph₄P⁺ = tetraphenylphosphonium cation]. These three known Mn^{III}-based SIMs exhibit an axial elongation because of the Jahn–Teller effect. Their axial ZFS parameters *D* were determined to be –3.3, –3.4, and –3.42 cm^{–1} by EPR (electron paramagnetic resonance) spectroscopy, and the effective energy barriers are 9.3, 7.8, and 12.6 cm^{–1}, respectively.^[11] More examples of six-coordinate Mn^{III} SIMs would reveal the correlation between structures and dynamic magnetic properties. Herein, we report the dynamic magnetic properties of three mononuclear Mn^{III} complexes with the chelating dibenzoylmethanido (dbm[–]) ligand, [Mn(dbm)₃] (**1**), [Mn(dbm)₂(L)₂](ClO₄) (L = DMSO = dimethyl sulfoxide, **2**; L = py = pyridine, **3**). These complexes show large, negative *D* values and field-induced slow magnetic relaxation. Complex **3** exhibits maxima of the out-of-phase ac susceptibility signals with energy barriers of *U*_{eff} = 18.5 cm^{–1}, which is a value higher than those in the three reported Mn-based SIMs.^[11]

Results and Discussion

Structures of **1–3** are presented in Figure 1. Crystallographic data, data collection and refinement parameters are listed in Table S1, and the corresponding bond lengths and angles around the Mn^{III} ions are given in Table 1. In **1**, the Mn^{III} ion is coordinated by three dbm[–] ligands, and the six oxygen atoms form a Jahn–Teller-distorted environment with an axial elongation along the O1–Mn–O4 direction (Figure 1, top). A similar coordination sphere was reported for [Mn{(OPPh₂)₂N}₃]^[11b,13] and [Mn(trop)₃].^[14] For **2**, the Mn^{III} ion is located in a six-coordinate octahedral environment with a static Jahn–Teller distortion, in which the four O donor atoms of two chelating dbm[–] ligands define the equatorial plane, whereas the remaining O atoms from two DMSO molecules reside in the axial positions (Figure 1, middle). The axial Mn–O bonds [2.169(3) and 2.177(3) Å] are longer than the equatorial Mn–O bonds [from 1.9061(18) to 1.9104(18) Å; average of 1.908 Å]. Moreover, the equatorial O–Mn–O bond angles are in the range 87.88(11)–91.96(8)°, which is close to the angle for an ideal octahedron (90°) (Table 1). The sulfur atom and one methyl group of each DMSO ligand are disordered at two positions. Two phenyl rings from the same dbm[–] ligand are nearly coplanar with a small twist angle of 7.84°. The structural features of **3** are similar to those of **2**. As in **2**, the coordinated atoms of the equatorial plane are provided by exactly two dbm[–] ligands, but the axially coordinated N atoms originate from two coordinated pyridine ligands (Figure 1, bottom). For one of the dbm[–] ligands, the dihedral angle between two phenyl rings is 51.60°, but the angle in the other dbm[–] ligand is 3.07°.

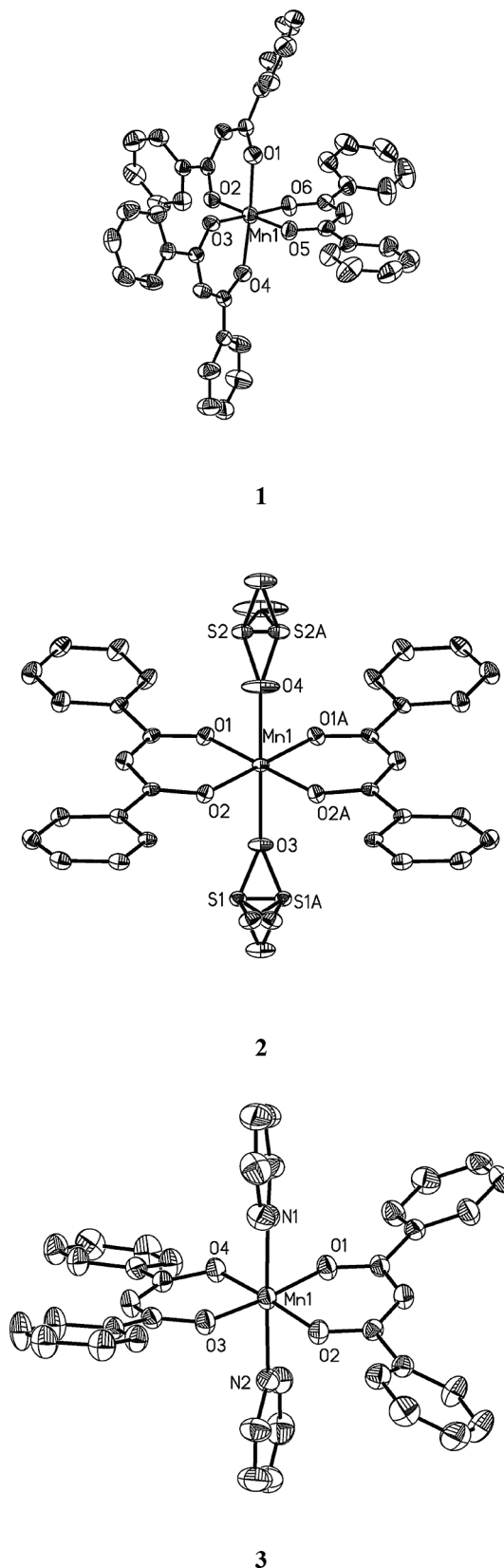


Figure 1. ORTEP drawings of **1** and the cations of **2** and **3**. H atoms are omitted for clarity.

As depicted in Table 1, the axially elongated Mn–O or Mn–N bonds for **1–3** are longer than the equatorial Mn–O

Table 1. Selected bond lengths [Å] and angles [°] for 1–3.

		1	2	3
Equatorial positions	Mn–O	1.902(3)	1.9061(18)	1.9025(16)
		1.927(3)	1.9061(18)	1.9117(16)
		1.929(3)	1.9104(18)	1.9130(16)
		1.941(3)	1.9104(18)	1.9195(15)
	O–Mn–O	87.90(14)	87.88(11)	87.35(7)
		88.74(14)	88.20(11)	89.12(7)
		90.61(15)	91.96(8)	91.59(7)
		92.74(14)	91.96(8)	92.37(7)
Axial positions	Mn–O/Mn–N	2.116(3)	2.169(3)	2.286(2)
		2.141(4)	2.177(3)	2.300(2)
	O–Mn–O/N–Mn–N	175.61(13)	177.96	178.77(8)

bonds, and the order of the axial bond lengths in the three complexes is $3 > 2 > 1$. The axial bond angles are almost perfectly linear. The sums (Σ) of the absolute values of deviation from 90° of the twelve *cis* angles for **1**, **2**, and **3** are 23.59° , 13.65° , and 27.14° , respectively, which indicates the small distortion from the ideal octahedron for the three complexes.^[15] To further estimate the degree of distortion, the continuous-shape-measurement (CSM) analysis was performed by using the SHAPE 2.1 program. The values obtained relative to the octahedron are 0.327, 0.418, and 0.931 for **1**, **2**, and **3**, respectively.^[15a,15b] Evidently, the deviation of **3** is the most significant. The closest intermolecular Mn–Mn distances for **1**, **2**, and **3** are 9.83(4), 7.69(9), and 8.28(5) Å, respectively, which indicates no close intermolecular exchange pathways.

The polycrystalline sample of **1–3** used for the magnetic measurements was characterized by powder X-ray diffraction analyses. The diffraction patterns are consistent with those calculated from the single-crystal X-ray diffraction data (Figures S1–S3, Supporting Information). Direct-current magnetic susceptibility measurements were carried out in the temperature range 1.8–300 K at 1 kOe (for **1** and **2**) and 2 kOe (for **3**), as shown in Figure 2. At room temperature, the $\chi_M T$ values for **1**, **2**, and **3** are 3.37 , 3.13 , and $2.96 \text{ cm}^3 \text{ K mol}^{-1}$, respectively, which is in agreement with an $S = 2$ spin center with g values of 2.12, 2.04, and 1.99, respectively. Upon lowering the temperature, the values of $\chi_M T$ remain relatively constant. Below approximately 50 K,

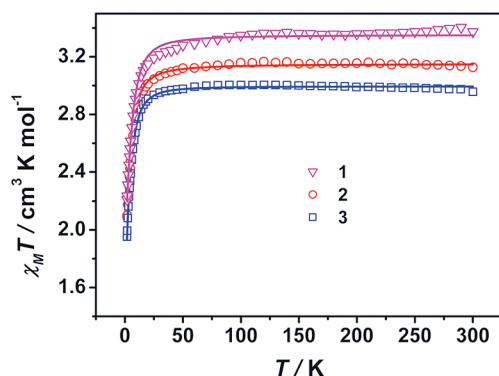


Figure 2. Variable-temperature dc susceptibility data of polycrystalline samples of **1–3**. Solid lines indicate the best fits obtained with the PHI program.^[16]

the values of $\chi_M T$ start to decrease and finally reach 2.21, 2.09, and $1.95 \text{ cm}^3 \text{ K mol}^{-1}$ at 1.8 K for **1**, **2**, and **3**, respectively. Because of the absence of close Mn \cdots Mn contacts in the crystal packing, the downturn below 50 K is most likely a result of the magnetic anisotropy of the Mn^{III} ions with $S = 2$ rather than of intermolecular interactions. Field-dependent magnetization measurements were performed between 1.8 and 5 K at applied magnetic fields in the range 1–7 T, as shown in Figures 3 and S4–S6. With increasing magnetic field, the magnetization for **1**, **2**, and **3** increases and reaches values of 3.28, 3.36, and $3.06 N\beta$, respectively, at 7 T. However, no saturation was achieved. The lack of saturation at 7 T and the non-superposition of M vs. H/T

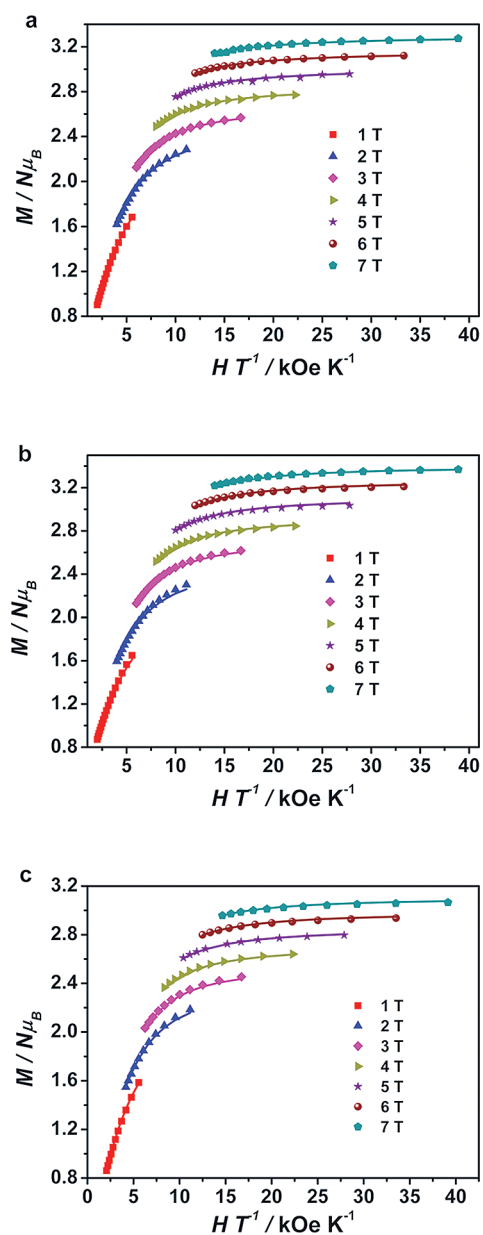


Figure 3. Variable-temperature, variable-field dc magnetization data collected on pure polycrystalline samples of **1** (a), **2** (b), and **3** (c). Fields of 1–7 T were used from 1.8 to 5 K. Solid lines indicate the best fits obtained with the PHI program.^[16]

curves further point to the presence of ZFS of the $S = 2$ ground state.

To evaluate the axial (D) and rhombic (E) ZFS parameters, the magnetic susceptibility and the magnetization data were simultaneously fit by using the PHI program^[16] and the anisotropic spin Hamiltonian given in Equation (1).

$$H = D[\hat{S}_z^2 - S(S + 1)/3] + E(\hat{S}_x^2 - \hat{S}_y^2) + \mu_B(g_x \hat{S}_x B_x + g_y \hat{S}_y B_y + g_z \hat{S}_z B_z) \quad (1)$$

Here, D and E represent the axial and rhombic ZFS parameters, and g_x , g_y , and g_z are the anisotropic g factors.

The best fits afforded the final parameters for **1–3** given in Table 2. It is clear that good agreement was achieved between the experimental and the simulated data for $\chi_M T$ vs. T (Figure 2) and M vs. H curves at various temperatures (Figure 3). It should be noted that **1** and **3** have been studied by Gatteschi et al.^[17] and Aromi et al.^[18] by using high-frequency and -field (HF) EPR spectroscopy, respectively. Evidently, the D and E values obtained here are consistent with the values determined by HF-EPR ($D = -4.35 \text{ cm}^{-1}$, $E = 0.28 \text{ cm}^{-1}$ for **1**; $D = -4.5 \text{ cm}^{-1}$, $E = -0.4 \text{ cm}^{-1}$ for **3**).

Table 2. Results of the fittings of the dc magnetic data carried out with the PHI program^[16] for **1–3**.

	g_z	$g_{x,y}$	D [cm^{-1}]	E [cm^{-1}]	Residual
1	2.03	2.16	-4.52	0.71	0.00013
2	1.92	2.11	-3.42	0.74	0.00041
3	1.97	2.01	-4.46	0.93	0.000047

To reveal the SMM characteristics of **1–3**, frequency-dependent alternating-current (ac) magnetic susceptibility was measured in the temperature range 1.8–10 K. No out-of-phase ac susceptibility (χ_M'') signal was observed under an applied dc field of zero for **1–3** (Figures S8–S10) because of the quantum tunneling of the magnetization (QTM) through the spin-reversal barrier. Hence, to reduce the QTM effect, a dc field of 1500 or 2000 Oe was employed in the ac measurements for **1–3**. As shown in Figure 4, with an applied dc field, only a frequency dependence of the χ_M'' signal was observed for **1** and **2**. However, obvious peaks of the χ_M'' signal appear for **3** at the frequencies in the range 250–1488 Hz with an applied dc field of 1500 Oe. The temperature and frequency dependence of the ac susceptibilities (Figures 4 and S11–S13) implies that all complexes exhibit SMM characteristics.

In the cases of **1** and **2**, because of the lack of observed peaks of the χ_M'' signal, the ac susceptibility data were treated by a model that assumes only single slow relaxation of magnetization by using the relationship $\ln(\chi_M''/\chi_M') = \ln(\omega\tau_0) + U_{\text{eff}}/k_B T$, where ω ($= 2\pi\nu$) is the frequency of the ac field, τ_0 is the pre-exponential factor, and U_{eff} is the effective energy barrier.^[19] The average values of U_{eff} are 11.5 cm^{-1} ($\tau_0 \approx 2.3 \times 10^{-7} \text{ s}$) and 16.8 cm^{-1} ($\tau_0 \approx 9.4 \times 10^{-9} \text{ s}$) for **1** and **2**, respectively (Figures 5 and 6). The τ_0 values obtained here are comparable to those found in SIMs based

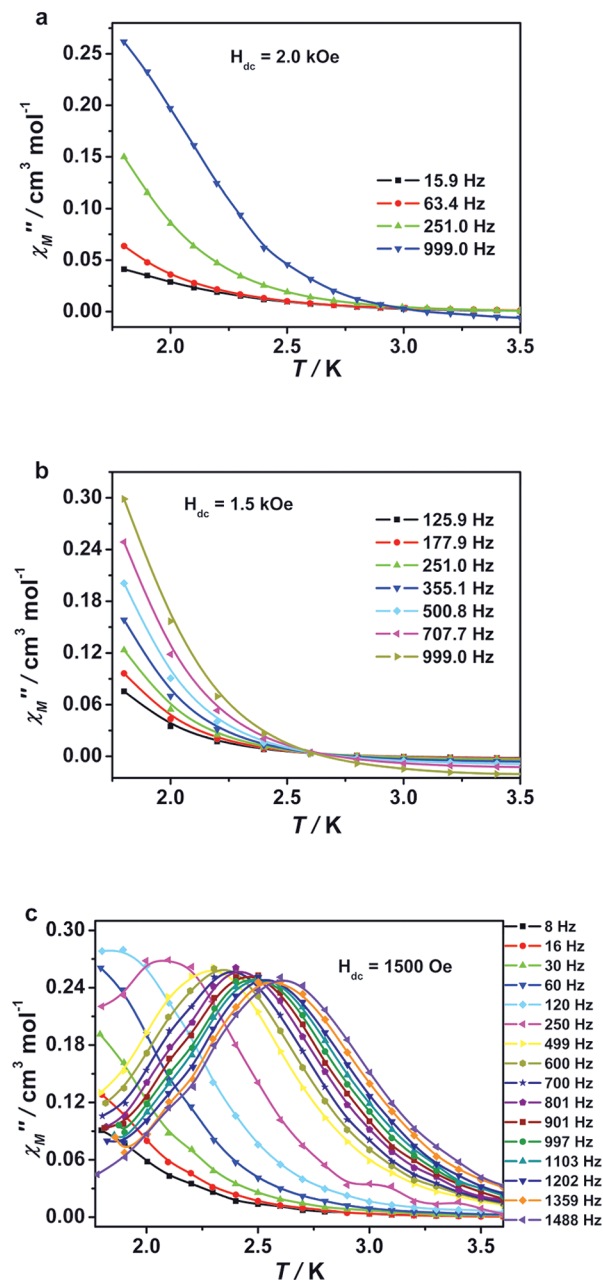


Figure 4. Temperature dependence of the out-of-phase ac magnetic susceptibility from 1.8 to 3.5 K under applied dc fields, measured on pure polycrystalline samples of **1** (a), **2** (b), and **3** (c). The solid lines are given as guide to the eye.

on transition metal ions.^[7–11] For **1**, the energy barrier ($4|D| = 18.2 \text{ cm}^{-1}$) calculated from HF-EPR data is considerably larger than the effective energy barrier (11.5 cm^{-1}), and this may be explained by the existence of non-negligible QTM. However, in **2**, the value of the energy barrier ($4|D| = 13.7 \text{ cm}^{-1}$) calculated from the dc magnetization measurements is smaller than the effective energy barrier 16.8 cm^{-1} . The latter value may have been overestimated and should be less than 13.7 cm^{-1} . This might reflect the limitation of the model used to evaluate the effective energy barriers, which assumes only single slow relaxation of magnetization. It should be noted that the presence of disorder in the

molecular structure of **2** likely results in multiple relaxation processes,^[20] which would render the model not appropriate.

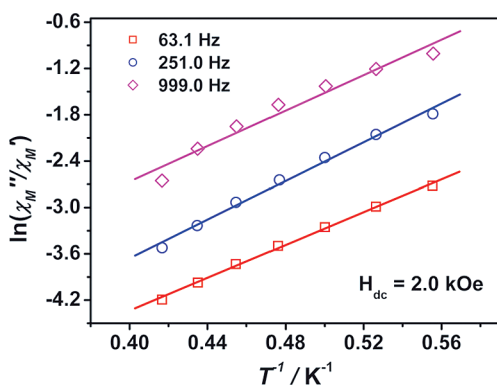


Figure 5. $\ln(\chi_M''/\chi_M')$ vs. T^{-1} plot and the best linear fits under the 2.0 kOe applied field for **1**.

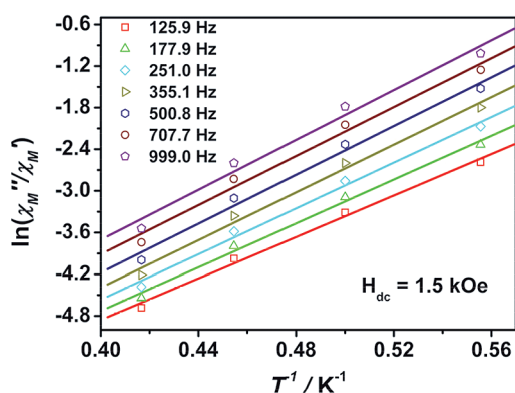


Figure 6. $\ln(\chi_M''/\chi_M')$ vs. T^{-1} plots and the best linear fits under the 1.5 kOe applied field for **2**.

For **3**, as depicted in Figure 4c, frequency-dependent maxima of the out-of-phase ac magnetic susceptibility were observed under a 1.5 kOe applied field. Cole–Cole plots were established and fitted by using the generalized Debye functions (Figure S14). The fitting parameters are summarized in Table S2 in the Supporting Information. The parameters a (a indicates the deviation from the pure Debye model) in the range 0.04–0.13 imply a narrow width of relaxation times. The Arrhenius plot, as depicted in Figure 7, was constructed by using the peaks of the out-of-phase χ_M'' signals from the temperature-dependent data at different frequencies (Figure 4c). A fit to the linear relationship affords the effective spin-reversal barrier of $U_{\text{eff}} = 18.5 \text{ cm}^{-1}$ ($\tau_0 = 9.2 \times 10^{-8}$). Only the thermally activated process was observed, which indicates that the QTM mediated by the hyperfine, dipolar interactions and the transverse anisotropy (E) is suppressed at the applied field of 1.5 kOe. It should be noted that the energy barrier in **3** is comparable to the value estimated from HFEP data ($4|D| = 18.0 \text{ cm}^{-1}$), which further implies that the applied field of 1.5 kOe fully suppresses the QTM effect.

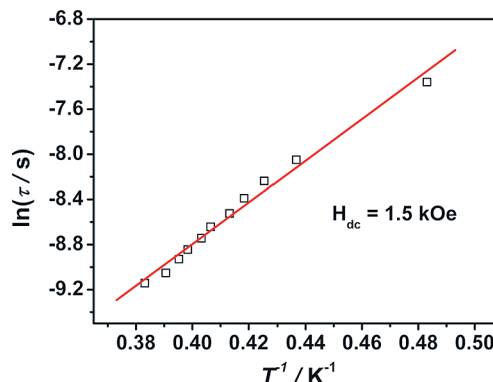


Figure 7. Relaxation time of the magnetization: $\ln(\tau)$ vs. T^{-1} plot at an applied field of 1.5 kOe for **3**. The solid lines represent Arrhenius fits. The data were derived from the maxima of χ_M'' vs. T at different frequencies.

The magnetic parameters of **1–3** and the three known Mn^{III} SIMs^[11] are listed in Table 3. The effective energy barrier of **3** (18.5 cm^{-1}) is significantly higher than those of the other Mn^{III} SIMs. The energy barriers U_{eff} for the field-induced slow magnetic relaxation vary with the dc field used.^[21] Therefore, the U_{eff} values are only compared if the same dc fields are used in the ac magnetic susceptibility measurements. The U_{eff} values of **1–3** and of the three reported Mn^{III} SIMs were obtained under different dc fields. However, careful examination of Table 3 could reveal some trends of the effective energy barriers. The effective barrier U_{eff} for these Mn^{III} SIMs seems to be influenced by the structural types and the ZFS parameters D . The six complexes could be divided into two types. One type, **1** and $[\text{Mn}\{(\text{OPPh}_2)_2\text{N}\}_3]$, has three chelating ligands. The other type, the remaining four complexes, contains chelating ligands and two monodentate ligands in the axial positions. In the two complexes of the first type, the larger U_{eff} value corresponds to the larger D value. A U_{eff} value of 11.5 cm^{-1} for **1** with a D value of -4.55 cm^{-1} is larger than 7.8 cm^{-1} for $[\text{Mn}\{(\text{OPPh}_2)_2\text{N}\}_3]$ with a D value of -3.4 cm^{-1} . Both U_{eff} values were obtained with the similar dc fields (2000 vs. 2250 Oe). The same trend is observed for complexes **2** and **3** of the second type. The U_{eff} value of **3** (18.5 cm^{-1}) obtained with a dc field of 1500 Oe is larger than that of **2** ($<13.7 \text{ cm}^{-1}$) under the same conditions. It is noteworthy that the magnetic parameters obtained so far are limited, and more experimental work is needed to reach a more reliable conclusion.

To further confirm our conclusions about the magnetic anisotropy obtained from the above magnetic analyses, Orca 3.02 calculations^[22] were performed with the generalized-gradient-approximation (GGA) PBE (Perdew–Burke–Ernzerhof)^[23] functional. This is a good choice, as confirmed by Neese et al.^[24] As expected, other functionals based on GGA yield very similar results and are therefore not reported. The spin–orbit coupling (SOC) operator used was the efficient implementation of the multicenter spin–orbit mean-field (SOMF) concept developed by Hess et al.^[25] The spin–spin contributions (SSC) to the D values

Table 3. Magnetic parameters for **1–3** and for the reported Mn^{III} SIMs.

Type	Complex	D [cm ⁻¹]	E [cm ⁻¹]	U_{eff} [cm ⁻¹]	τ_o [s]	H_{dc} [Oe] ^[a]	Ref.
1	[Mn(dbm) ₃] (1)	-4.55 ^[b]	0.28 ^[b]	11.5	2.3×10^{-7}	2000	this work
	[Mn{(OPPh ₂) ₂ N} ₃]	-3.4 ^[b]		7.8	8.2×10^{-8}	2250	[12b]
2	[Mn(dbm) ₂ (DMSO) ₂] (2)	-3.42 ^[c]	0.74 ^[c]	16.8 ^[d]	9.4×10^{-9}	1500	this work
	[Mn(dbm) ₂ (pyridine) ₂] (3)	-4.5 ^[b]	-0.40 ^[b]	18.5	9.2×10^{-8}	1500	this work
	[Mn{5-TMAM(<i>R</i>)-salmen}(H ₂ O)Co(CN) ₆]	-3.3 ^[b]	0 ^[b]	9.3	8.0×10^{-8}	0	[12a]
	(Ph ₄ P)[Mn(opbaCl ₂)(py) ₂]	-3.42 ^[b]	-0.15 ^[b]	12.6	1.24×10^{-7}	1000	[11c]

[a] The applied fields used for ac magnetic susceptibility measurements. [b] Obtained by HFEPFR spectroscopy. [c] Obtained by fitting the dc magnetic data. [d] This value was overestimated and should be less than 13.7 cm⁻¹.

were also included, although they are very small for our complexes.^[24] The coupled-perturbed (CP) method proposed by Neese,^[24] which uses revised prefactors for the spin-flip terms and solves a set of coupled perturbed equations for the SOC perturbation, was used. CASSCF (complete active space self-consistent field) calculations with four electrons in the five Mn 3d-based orbitals [CAS(4,5)], spectroscopy-oriented CI (SORCI),^[26] and difference-dedicated configuration interaction (DDCI3)^[27] on top of the CAS(4,5) reference states were carried out. In the calculations, the orbitals were determined for the average of 5 $S = 2$ and 45 $S = 1$ roots. All calculations were performed with triple- ζ and one polarization function TZVP^[28] basis set for all atoms. Tight convergence criteria were used to ensure that the results are well converged with respect to technical parameters. In the above calculations of D and E employing SORCI and DDCI3, the SOC and SSC contributions were both included. The calculated values of the ZFS parameters for **1–3** are shown in Table 4, and they agree with the values obtained from analysis of the dc magnetic data. Furthermore, the magnetic anisotropic axis, calculated by using DDCI3, locates the axial Mn–L bond (Figure S7), and indicates that the ligand field exhibits higher axial character in the axial direction.

Table 4. Calculated and experimental D , E [cm⁻¹], and g values (x , y , z) for the ground state of complexes **1–3** obtained by using PBE, SORCI, and DDCI3.

	PBE		SORCI		DDCI3		$g^{\text{[a]}}$
	D	E	D	E	D	E	
1	-2.45	0.08	-3.35	0.06	-4.07	0.05	1.995, 1.992, 1.965
2	-2.03	0.09	-3.03	0.06	-3.64	0.01	1.994, 1.994, 1.969
3	-2.60	0.13	-3.66	0.01	-3.95	0.01	1.995, 1.994, 1.969

[a] Obtained by DDCI3.

From Table 4, the D values of **1–3** calculated by using DDCI3 are closest to the experimental values. The structures of **2** and **3** are very similar, but their D values are somewhat different. We wondered whether the pyridine ligands in **3** lead to the larger D value compared to the DMSO ligands in **2**. To investigate this, we used two pyridine ligands to substitute two DMSO molecules in **2** and to obtain a model molecule **2a**. The distances Mn–N in **2a** are the same as those in **3**. The D value of **2a** calculated by using DDCI3 is -3.94 cm⁻¹, which is almost the same as that of **3**. Thus, we believe that the pyridine ligands around

Mn^{III} in **3** are responsible for its larger D value compared to **2**.

Conclusions

We have described the magnetic properties of three mononuclear Mn^{III} complexes with octahedral coordination environments. The ZFS parameters D for **1–3** were determined by fitting the magnetic susceptibility and the magnetization data. The large negative D values are consistent with the Jahn–Teller axis elongation of the octahedral geometry. Complexes **1–3** show frequency dependence of their ac susceptibility under applied dc fields. Maxima of the out-of-phase ac susceptibility signals are observed in **3**. The effective spin-reversal barrier of $U_{\text{eff}} = 18.5$ cm⁻¹ for **3** is higher than those of the other Mn^{III} SIMs. Possible reasons for the dynamic properties of **1–3** were discussed. A more reliable relationship between the structure and the magnetic properties requires additional studies of other Mn^{III} SIMs.

Experimental Section

General: Unless otherwise stated, all chemicals were purchased from commercial sources and used without further purification. *n*Bu₄NMnO₄ was prepared as previously reported.^[29] [Mn(dbm)₃] (**1**), [Mn(dbm)₂(L)₂](ClO₄) (L = DMSO, **2**; L = py, **3**) were prepared according to a modified method of Aromi et al., which was originally used to prepare **3**.^[18] Elemental analyses were performed with an Elementar Vario ELIII elemental analyzer. The powder XRD patterns were measured at room temperature with a Bruker D8 Advance X-ray diffractometer.

Synthesis of [Mn(dbm)₃] (1**):** To a solution of Mn(ClO₄)₂·6H₂O (0.225 g, 0.62 mmol) in acetonitrile (10 mL) was slowly added a purple solution of *n*Bu₄NMnO₄ (0.055 g, 0.15 mmol) in acetonitrile (2 mL). Solid Hdbm (0.42 g, 1.86 mmol) was added, and the mixture was stirred for 10 min and then filtered. The filtrate was left in a beaker until crystallization started and afforded dark crystals. The yield was 56% with respect to Mn. C₄₅H₃₃MnO₆ (724.69): calcd. C 74.58, H 4.59; found C 74.29, H 4.74.

Synthesis of [Mn(dbm)₂(DMSO)₂](ClO₄) (2**):** To a yellowish solution of Mn(ClO₄)₂·6H₂O (0.225 g, 0.62 mmol) and DMSO (1.0 mL, 11.6 mmol) in acetonitrile (10 mL) was slowly added a purple solution of freshly prepared *n*Bu₄NMnO₄ (0.055 g, 0.15 mmol) in acetonitrile (2 mL). Solid Hdbm (0.35 g, 1.55 mmol) was added immediately to the resulting dark brown solution, and the mixture was stirred for a few hours and then filtered. The filtrate was kept

in a beaker until crystallization occurred. Red-brown crystals were isolated with a yield of 20% with respect to Mn. $C_{34}H_{32}ClMnO_{10}S_2$ (755.13); calcd. C 54.08, H 4.27; found C 53.85, H 4.59.

Synthesis of $[Mn(dbm)_2(py)_2](ClO_4)$ (3): The complex was prepared by using the same procedure as for complex **2**, but with pyridine (1.5 mL, 18.5 mmol) instead of dimethyl sulfoxide (1 mL, 11.6 mmol). Dark brown crystals were obtained. The yield was 34% with respect to Mn. $C_{40}H_{32}ClMnN_2O_8$ (759.09); calcd. C 63.29, H 4.25, N 3.69; found C 63.21, H 4.63, N 3.43.

X-ray Structure Determination: Single-crystal X-ray diffraction data for **1–3** were collected with a Bruker APEX DUO diffractometer with a CCD area detector by using graphite-monochromated Mo- K_α radiation ($\lambda = 0.71073 \text{ \AA}$) at room temperature.^[30] The APEXII program was used for collecting frames of data and determining lattice parameters. Data were integrated with the SAINT program. Absorption corrections were applied by using SADABS.^[31] The structures of complexes **1–3** were solved with the program SHELXS-97 and subsequently completed by using the full-matrix least-squares technique with the SHELXL 97 program.^[32] The positions of Mn and Cl atoms were easily determined, and S, O, N, and C atoms were subsequently identified by using difference Fourier maps. All non-hydrogen atoms were refined with anisotropic displacement parameters. Hydrogen atoms on organic ligands were set in calculated positions and generated by the riding model. The structures of complexes **1**^[17,33] and **3**^[18] were previously reported, but we recollected the data on our own samples to confirm their structures. CCDC-1017697 (for **2**), -1018575 (for **3**), and 1018576 (for **1**) contain the supplementary crystallographic data for this paper. These data can be obtained free of charge from The Cambridge Crystallographic Data Centre via www.ccdc.cam.ac.uk/data_request/cif.

Magnetic Measurements: The magnetic properties were recorded at fields up to 7 T between 1.8 and 300 K with a Quantum Design SQUID VSM magnetometer (for **1** and **2**) at 1 kOe and with a Quantum Design MPMS-XL17 SQUID instrument (for **3**) at 2 kOe. The temperature- and frequency-dependent ac susceptibility data were collected by using an oscillating ac field of 2.0 Oe and ac frequencies ranging from 1 to 1000 Hz for **1** and **2**, whereas an oscillating ac field of 5.0 Oe and ac frequencies ranging from 1 to 1500 Hz were used for **3**. The magnetic susceptibility data were corrected for the sample holder as well as for diamagnetism of the constituent atoms (estimated by using Pascal constants).

Supporting Information (see footnote on the first page of this article): Parameters of crystal data collection and refinement, experimental and calculated powder XRD patterns, magnetization measurements, frequency- and temperature-dependent ac susceptibility data, and Cole–Cole plots.

Acknowledgments

We are grateful for the financial support from the National Basic Research Program of China (No. 2013CB922102 to X.-T. C. and Y. S.) and from the Priority Academic Program for the Development of Jiangsu Higher Education Institutions (to Y.-Q. Z.). The donors of the American Chemical Society Petroleum Research Fund are also acknowledged for partial support of this research (to Z.-L. X.).

[1] a) G. Christou, D. Gatteschi, D. N. Hendrickson, R. Sessoli, *MRS Bull.* **2000**, 25, 66–71; b) D. Gatteschi, R. Sessoli, J. Villain, *Molecular Nanomagnets*, Oxford University Press, Oxford,

2006; c) R. Winpenny, *Molecular Cluster Magnets*, World Scientific, Singapore, **2012**.

- [2] a) R. Sessoli, H. L. Tsai, A. R. Schake, S. Wang, J. B. Vincent, K. Folting, D. Gatteschi, G. Christou, D. N. Hendrickson, *J. Am. Chem. Soc.* **1993**, 115, 1804; b) S. M. J. Aubin, M. W. Wemple, D. M. Adams, H.-L. Tsai, G. Christou, D. N. Hendrickson, *J. Am. Chem. Soc.* **1996**, 118, 7746; c) G. Aromí, S. M. J. Aubin, M. A. Bolcar, G. Christou, H. J. Eppley, K. Folting, D. N. Hendrickson, J. C. Huffman, R. C. Squire, H.-L. Tsai, S. Wang, M. W. Wemple, *Polyhedron* **1998**, 17, 3005; d) G. Christou, *Polyhedron* **2005**, 24, 2065; e) O. Roubeau, R. Clérac, *Eur. J. Inorg. Chem.* **2008**, 4325; f) G. Aromí, E. K. Brechin, *Struct. Bond* **2006**, 122, 1–67.
- [3] a) R. E. P. Winpenny, *Chem. Soc. Rev.* **1998**, 27, 447; b) M. Sakamoto, K. Manseki, H. Ōkawa, *Coord. Chem. Rev.* **2001**, 219–221, 379; c) S. Tanase, J. Reedijk, *Coord. Chem. Rev.* **2006**, 250, 2501; d) M. Andruh, J.-P. Costes, C. Diaz, S. Gao, *Inorg. Chem.* **2009**, 48, 3342; e) J. W. Sharples, D. Collison, *Coord. Chem. Rev.* **2014**, 260, 1; f) H. L. C. Feltham, S. Brooker, *Coord. Chem. Rev.* **2014**, 276, 1.
- [4] a) R. Sessoli, A. K. Powell, *Coord. Chem. Rev.* **2009**, 253, 2328; b) Y.-N. Guo, G.-F. Xu, Y. Guo, J. K. Tang, *Dalton Trans.* **2011**, 40, 9953; c) P. Zhang, Y.-N. Guo, J. K. Tang, *Coord. Chem. Rev.* **2013**, 257, 1728; d) F. Habib, M. Murugesu, *Chem. Soc. Rev.* **2013**, 42, 3278.
- [5] N. Ishikawa, M. Sugita, T. Ishikawa, S. Koshihara, Y. Kaizu, *J. Am. Chem. Soc.* **2003**, 125, 8694.
- [6] a) D. N. Woodruff, R. E. P. Winpenny, R. A. Layfield, *Chem. Rev.* **2013**, 113, 5110; b) P. Zhang, L. Zhang, C. Wang, S.-F. Xue, S.-Y. Lin, J. K. Tang, *J. Am. Chem. Soc.* **2014**, 136, 4484.
- [7] a) J. M. Zadrozny, J. R. Long, *J. Am. Chem. Soc.* **2011**, 133, 20732; b) T. Jurca, A. Farghal, P.-H. Lin, I. Korobkov, M. Murugesu, D. S. Richeson, *J. Am. Chem. Soc.* **2011**, 133, 15814; c) J. M. Zadrozny, J. J. Liu, N. A. Piro, C. J. Chang, S. Hill, J. R. Long, *Chem. Commun.* **2012**, 48, 3897; d) A. Buchholz, A. O. Eseola, W. Plass, C. R. Chimie, **2012**, 15, 929; e) J. Vallejo, I. Castro, R. Ruiz-García, J. Cano, M. Julve, F. Lloret, G. D. Munno, W. Wernsdorfer, E. Pardo, *J. Am. Chem. Soc.* **2012**, 134, 15704; f) S. Gomez-Coca, E. Cremades, N. Aliaga-Alcalde, E. Ruiz, *J. Am. Chem. Soc.* **2013**, 135, 7010; g) F. Yang, Q. Zhou, Y. Q. Zhang, G. Zeng, G. H. Li, Z. Shi, B. W. Wang, S. H. Feng, *Chem. Commun.* **2013**, 49, 5289; h) D.-K. Cao, J.-Q. Feng, M. Ren, Y.-W. Gu, Y. Song, M. D. Ward, *Chem. Commun.* **2013**, 49, 8863; i) J. M. Zadrozny, J. Telsler, J. R. Long, *Polyhedron* **2013**, 64, 209; j) W. Huang, T. Liu, D. Y. Wu, J. J. Cheng, Z. W. Ouyang, C. Y. Duan, *Dalton Trans.* **2013**, 42, 15326; k) F. Habib, O. R. Luca, V. Vieru, M. Shiddiq, I. Korobkov, S. I. Gorelsky, M. K. Takase, L. F. Chibotaru, S. Hill, R. H. Crabtree, M. Murugesu, *Angew. Chem. Int. Ed.* **2013**, 52, 11290; *Angew. Chem.* **2013**, 125, 11500; l) Y.-Y. Zhu, C. Cui, Y.-Q. Zhang, J.-H. Jia, X. Guo, C. Gao, K. Qian, S.-D. Jiang, B.-W. Wang, Z.-M. Wang, S. Gao, *Chem. Sci.* **2013**, 4, 1802; m) V. Chandrasekhar, A. Dey, A. J. Mota, E. Colacio, *Inorg. Chem.* **2013**, 52, 4554; n) E. Colacio, J. Ruiz, E. Ruiz, E. Cremades, J. Krzystek, S. Carretta, J. Cano, T. Guidi, W. Wernsdorfer, E. K. Brechin, *Angew. Chem. Int. Ed.* **2013**, 52, 9130; *Angew. Chem.* **2013**, 125, 9300; o) D. Y. Wu, X. X. Zhang, P. Huang, W. Huang, M. Y. Ruan, Z. W. Ouyang, *Inorg. Chem.* **2013**, 52, 10976; p) R. Herchel, L. Váhovská, I. Potočňák, Z. Trávníček, *Inorg. Chem.* **2014**, 53, 5896; q) A. Eichhofer, Y. Lan, V. Mereacre, T. Bodenstein, F. Weigend, *Inorg. Chem.* **2014**, 53, 1962; r) R. Boča, J. Miklovič, J. Titiš, *Inorg. Chem.* **2014**, 53, 2367; s) P. Cucus, F. Tuna, L. Sorace, I. Matei, C. Maxim, S. Shova, R. Gheorghie, A. Caneschi, M. Hillebrand, M. Andruh, *Inorg. Chem.* **2014**, 53, 7738; t) M. R. Saber, K. R. Dunbar, *Chem. Commun.* **2014**, 50, 12266; u) M. S. Fataftah, J. M. Zadrozny, D. M. Rogers, D. E. Freedman, *Inorg. Chem.* **2014**, 53, 10716; v) L. Chen, J. Wang, J.-M. Wei, W. Wernsdorfer, X.-T. Chen, Y.-Q. Zhang, You Song, Z.-L. Xue, *J. Am. Chem. Soc.* **2014**, 136, 12213.

- [8] a) J. M. Zadrozny, D. J. Xiao, M. Atanasov, G. J. Long, F. Grandjean, F. Neese, J. R. Long, *Nat. Chem.* **2013**, *5*, 577; b) P. P. Samuel, K. C. Mondal, N. A. Sk, H. W. Roesky, E. Carl, R. Neufeld, D. Stalke, S. Demeshko, F. Meyer, L. Ungur, L. F. Chibotaru, J. Christian, V. Ramachandran, J. van Tol, *J. Am. Chem. Soc.* **2014**, *136*, 11964; c) J. M. Zadrozny, M. Atanasov, A. M. Bryan, C.-Y. Lin, B. D. Rekker, P. P. Power, F. Neese, J. R. Long, *Chem. Sci.* **2013**, *4*, 125; d) P.-H. Lin, N. C. Smythe, S. I. Gorelsky, S. Maguire, N. J. Henson, I. Korobkov, B. L. Scott, J. C. Gordon, R. T. Baker, M. Murugesu, *J. Am. Chem. Soc.* **2011**, *133*, 15806; e) D. E. Freedman, W. H. Harman, T. D. Harris, G. J. Long, C. J. Chang, J. R. Long, *J. Am. Chem. Soc.* **2010**, *132*, 1224; f) W. H. Harman, T. D. Harris, D. E. Freedman, H. Fong, A. Chang, J. D. Rinehart, A. Ozarowski, M. T. Sougrati, F. Grandjean, G. J. Long, J. R. Long, C. J. Chang, *J. Am. Chem. Soc.* **2010**, *132*, 18115; g) D. Weismann, Y. Sun, Y. Lan, G. Wolmershäuser, A. K. Powell, H. Sitzmann, *Chem. Eur. J.* **2011**, *17*, 4700; h) C. Mathonière, H.-J. Lin, D. Siretanu, R. Clérac, J. M. Smith, *J. Am. Chem. Soc.* **2013**, *135*, 19083; i) X. Feng, C. Mathonière, I.-R. Jeon, M. Rouzières, A. Ozarowski, M. L. Aubrey, M. I. Gonzalez, R. Clérac, J. R. Long, *J. Am. Chem. Soc.* **2013**, *135*, 15880; j) S. Mossin, B. L. Tran, D. Adhikari, M. Pink, F. W. Heinemann, J. Sutter, R. K. Szilagyi, K. Meyer, D. J. Mindiola, *J. Am. Chem. Soc.* **2012**, *134*, 13651.
- [9] R. C. Poulten, M. J. Page, A. G. Algarra, J. J. Le Roy, I. Lopez, E. Carter, A. Llobet, S. A. Macgregor, M. F. Mahon, D. M. Murphy, M. Murugesu, M. K. Whittlesey, *J. Am. Chem. Soc.* **2013**, *135*, 13640.
- [10] a) J. Martínez-Lillo, T. F. Mastropietro, E. Lhotel, C. Paulsen, J. Cano, G. De Munno, J. Faus, F. Lloret, M. Julve, S. Nellutla, J. Krzystek, *J. Am. Chem. Soc.* **2013**, *135*, 13737; b) K. S. Pedersen, M. Sigrist, M. A. Soensen, A.-L. Barra, T. Weyhermüller, S. Piligkos, C. A. Thuesen, M. G. Vinum, H. Mutka, H. Weihe, R. Clerac, J. Bendix, *Angew. Chem. Int. Ed.* **2014**, *53*, 1351; *Angew. Chem.* **2014**, *126*, 1375.
- [11] a) R. Ishikawa, R. Miyamoto, H. Nojiri, B. K. Breedlove, M. Yamashita, *Inorg. Chem.* **2013**, *52*, 8300; b) A. Grigoropoulos, M. Pissas, P. Papatolis, V. Psycharis, P. Kyritsis, Y. Sanakis, *Inorg. Chem.* **2013**, *52*, 12869; c) J. Vallejo, A. Pascual-Álvarez, J. Cano, I. Castro, M. Julve, F. Lloret, J. Krzystek, G. D. Munno, D. Armentano, W. Wernsdorfer, R. Ruiz-García, E. Pardo, *Angew. Chem. Int. Ed.* **2013**, *52*, 14075; *Angew. Chem.* **2013**, *125*, 14325.
- [12] a) J. Krzystek, G.-J. Yeagle, J.-H. Park, R.-D. Britt, M.-W. Meisel, L.-C. Brunel, J. Telsler, *Inorg. Chem.* **2003**, *42*, 4610; b) J. Krzystek, A. Ozarowski, J. Telsler, *Coord. Chem. Rev.* **2006**, *250*, 2308.
- [13] N. Zuniga-Villareal, M. Reyes Lezama, S. Hernandez-Ortega, C. Silvestru, *Polyhedron* **1998**, *17*, 2679.
- [14] A. Avdeef, J. A. Costamagna, J. P. Fackler, *Inorg. Chem.* **1974**, *13*, 1854.
- [15] a) S. Alvarez, P. Alemany, D. Casanova, J. Cirera, M. Llunell, D. Avnir, *Coord. Chem. Rev.* **2005**, *249*, 1693; b) S. Alvarez, D. Avnir, M. Llunell, M. Pinsky, *New J. Chem.* **2002**, *26*, 996; c) P. Guionneau, M. Marchivie, G. Bravic, J.-F. Létard, D. J. Chasseau, *J. Mater. Chem.* **2002**, *12*, 2546.
- [16] N. F. Chilton, R. P. Anderson, L. D. Turner, A. Soncini, K. S. Murray, *J. Comput. Chem.* **2013**, *34*, 1164.
- [17] A.-L. Barra, D. Gatteschi, R. Sessoli, G. L. Abbati, A. Cornia, A. C. Fabretti, M. G. Uytterhoeven, *Angew. Chem. Int. Ed. Engl.* **1997**, *36*, 2329; *Angew. Chem.* **1997**, *109*, 2423.
- [18] G. Aromi, J. Telsler, A. Ozarowski, L.-C. Brunel, H.-M. Stoeckli-Evans, J. Krzystek, *Inorg. Chem.* **2005**, *44*, 187.
- [19] J. Bartolomé, G. Filoti, V. Kuncser, G. Schinteie, V. Mereacre, C. E. Anson, A. K. Powell, D. Prodius, C. Turta, *Phys. Rev. B* **2009**, *80*, 014430.
- [20] S.-D. Jiang, B.-W. Wang, H.-L. Sun, Z.-M. Wang, S. Gao, *J. Am. Chem. Soc.* **2011**, *133*, 4730.
- [21] J. Martínez-Lillo, D. Armentano, G. D. Munno, W. Wernsdorfer, M. Julve, F. Lloret, J. Faus, *J. Am. Chem. Soc.* **2006**, *128*, 14218.
- [22] F. Neese, *ORCA – An Ab Initio, Density Functional and Semi-empirical Program Package*, Version 3.02, Max-Planck Institute for Bioinorganic Chemistry, Mülheim an der Ruhr, Germany, **2014**.
- [23] J. P. Perdew, K. Burke, M. Ernzerhof, *Phys. Rev. Lett.* **1996**, *77*, 3865.
- [24] a) F. Neese, *J. Chem. Phys.* **2007**, *127*, 164112; b) M. R. Pederson, S. Khanna, *Phys. Rev. B* **1999**, *60*, 9566; c) J. Kortus, M. R. Pederson, T. Baruah, N. Bernstein, C. S. Hellberg, *Polyhedron* **2003**, *22*, 1871; d) J. Ribas-Arino, T. Baruah, M. R. Pederson, *J. Am. Chem. Soc.* **2006**, *128*, 9497.
- [25] B. A. Hess, C. M. Marian, U. Wahlgren, O. Gropen, *Chem. Phys. Lett.* **1996**, *251*, 365.
- [26] F. Neese, *J. Chem. Phys.* **2003**, *119*, 9428.
- [27] J. Miralles, O. Castell, R. Caballol, J. P. Malrieu, *Chem. Phys. Lett.* **1993**, *172*, 33.
- [28] F. Weigend, R. Ahlrichs, *Phys. Chem. Chem. Phys.* **2005**, *7*, 3297.
- [29] J. B. Vincent, K. Foltling, J. C. Huffman, G. Christou, *Inorg. Chem.* **1996**, *35*, 996.
- [30] *SMART & SAINT*, Software Reference Manuals, version 6.45, Bruker Analytical X-ray Systems, Inc., Madison, WI, **2003**.
- [31] G. M. Sheldrick, *SADABS – Software for Empirical Absorption Correction*, version 2.05, University of Göttingen, Göttingen, Germany, **2002**.
- [32] G. M. Sheldrick, *SHELXL97 – Program for Crystal Structure Refinement*, University of Göttingen, Göttingen, Germany, **1997**.
- [33] E. G. Zaitseva, I. A. Baidina, P. A. Stabnikov, S. V. Borisov, L. K. Igumenov, *Zh. Strukt. Khim.* **1990**, *31*, 184 (*Chem. Abstr.* **1990**, *113*, 88602h).

Received: October 9, 2014

Published Online: ■

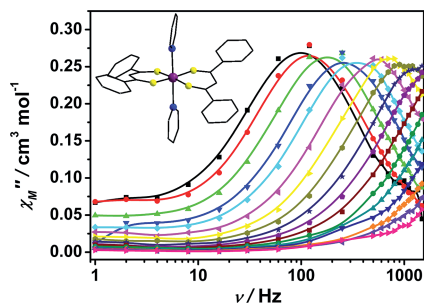
Slow Magnetic Relaxation

L. Chen, J. Wang, Y.-Z. Liu, Y. Song,
X.-T. Chen,* Y.-Q. Zhang,*
Z.-L. Xue 1–9



Slow Magnetic Relaxation in Mononuclear Octahedral Manganese(III) Complexes with Dibenzoylmethanide Ligands

Keywords: Manganese / N,O ligands / Single-molecule magnets / Magnetic properties



Three mononuclear Mn^{III} complexes based on the dibenzoylmethanido ligand and having negative zero-field-splitting parameters *D* exhibit field-induced slow relaxation behavior.